Heat transfer and second order slip effect on MHD flow of fractional Maxwell fluid in a porous medium

Sidra Aman [a], Qasem Al-Mdallal [a,*], Ilyas Khan [b]

[a] *Department of Mathematical Sciences, UAE University, P.O Box 15551, Al-Ain, United Arab Emirates*
[b] *Basic Engineering Science Department, College of Engineering, Majmaah University, Saudi Arabia*

ARTICLE INFO

ABSTRACT

This work explores the effect of second order slip on magnetohydrodynamic (MHD) flow of a fractional Maxwell fluid on a moving plate and a comparison between two numerical algorithms (Tzou and Stehfest's algorithm). The problem is formulated for Maxwell fluid with Caputo-time fractional derivatives. Semi analytical solutions are derived using Laplace transform. The solution is obtained using numerical technique of Laplace transform Stehfest's algorithm. To insight the physical behavior of the fluid, a graphical illustration is made. The influence of fractional parameter, the magnetic force, the porosity parameter, the slip parameters are analyzed and discussed. A tabular and graphical comparisons with Tzou's algorithm are made for the sake of validation of the present results.

1. Introduction

The viscoelastic fluids pass through many incidents in industry and engineering, such as synthetic propellants, polymer solutions and many others. Maxwell fluid has been studied widely among all the viscoelastic fluid models (Fetecau and Fetecau, 2004; Fetecau et al., 2009; Tan and Masuoka, 2007; Jamil et al., 2011; Abbasbandy et al., 2014; Aman et al., 2017a,b). The flow of Maxwell fluid is important to industrial applications. A Peristaltic motion of Maxwell fluid was examined by Abbasi et al. (2016). Hsiao (2014) had examined Maxwell fluid flow using Numerical Method. Aman et al. (2017a,b) studied Maxwell nanofluid with four types of molecular liquids. Hsiao (2017) studied Maxwell fluid electrical MHD thermal extrusion system with viscous dissipation. It was a minor implementation to thermal extrusion manufacturing processing system energy.

Viscoelastic behavior is described by the constitutive equations with fractional derivatives. These fractional derivatives are acquired from the classical derivatives. The generalization of the classical to fractional dynamics is acquired by utilizing some approaches of fractional derivatives. Formal Caputo or Riemann-Liouville differential operators are used widely in engineering (Ruzhansky et al., 2017; Baltaeva and Agarwal, 2018; Agarwal et al., 2017). Caputo-Fabrizio is one of the modern approaches established by Caputo and Fabrizio (2015) which is appropriate for Laplace transform. Shah et al. (2017) examined flow of a fractional fluid over a vertical plate. They obtained a semi analytical solution for the Laplace inverse. Siddique and Vieru (2011) investigated stokes flow of a Newtonian fluid with fractional derivatives under the slip condition. Atangana (2016) used fractional derivative to non-linear Fisher's reaction-diffusion equation. Aman et al. (2018a,b) used Caputo time fractional model for heat transfer enhancement of water-based graphene nanofluid. Al-Mdallal et al. (2010) investigated fractional boundary value problems via numerical approach collocation-shooting method. Some important literature concerning the numerical approaches in fractional and discrete fractional calculus can be found in (Abdeljawad and Baleanu, 2017; Abdeljawad and Baleanu, 2016; Abu-Saris and Al-Mdallal, 2013; Al-Mdallal and Syam, 2012; Al-Mdallal and Hajji, 2015; Aman et al., 2018a,b) and the references therein.

Flow of non-Newtonian fluids with porous medium has been reported in many biological and industrial processes. Abbas et al. (2006) studied MHD flow of Maxwell fluid in a porous channel. Hayat et al. (2011) studied MHD flow of Maxwell fluid in a channel with porous medium. Tripathi and Bég (2012) investigated numerically the oscillating peristaltic flow of generalized Maxwell fluid using homotopy perturbation method.

Two types of slip conditions are generally considered in fluid problems namely slip and no-slip boundary conditions. In the no-slip boundary conditions there is no relative motion between walls and fluid but there are some surfaces where the liquids slip against the walls. For example, in the capillaries the no-slip condition doesn't work (Day, 1990). Thus, the no-slip condition is inadequate in several situations such as flow of polymeric liquids. In addition, slip condition also named as Navier condition has a remarkable importance in lubrication, medical sciences, polishing artificial heart valves and biological fluids. Maxwell fluid is analyzed with slip condition for Couette and stokes' flow (Ebaid, 2008; Vieru and Rauf, 2011; Vieru and Zafar, 2013). Hayat et al. (2016) analyzed unsteady MHD flow over exponentially stretching sheet with slip conditions. Ishak et al. (2017) used slip condition while studying Maxwell fluid stagnation point flow numerically. Fractional Maxwell fluid is studied by Liu and Guo (2017) and Tahir et al. (2017) with second-order slip.

The above literature motivated us to examine the heat, velocity and shear stress for the flow of Fractional Maxwell fluid with second order slip in a porous medium. The constitutive equations are formulated using fractional calculus. The semi analytical solutions are obtained using Laplace transform and Numerical Laplace inverse transform (Stehfest's and Tzou's algorithms). Moreover, the results obtained from both algorithms are compared numerically and graphically for the sake of validity.

2. Preliminary

In this section, we present some information about Caputo-Fabrizio fractional derivative and its properties:

Definition 1: Let $f \in H^1(a,b), b > a, alpha \in [0,1]$ then the new Caputo-Fabrizio fractional derivative is defined as:

$$D_t^\alpha f(t) = \frac{\alpha M(\alpha)}{(1-\alpha)} \int_a^t e^{\left(\frac{-\alpha(t-\tau)}{(1-\alpha)}\right)} \frac{\partial f(\tau)}{\partial \tau} d\tau \qquad (1)$$

where $M(\alpha) = a$ is the normalization function satisfying $M(0) = M(1) = 1$; for more details the reader is referred to Caputo and Fabrizio (2015). However; if $f \notin H^1(a,b)$, then the derivative becomes:

$$D_t^\alpha f(t) = \frac{\alpha M(\alpha)}{(1-\alpha)} \int_a^t e^{\left(\frac{-\alpha(t-\tau)}{(1-\alpha)}\right)} [f(t) - f(\tau)] d\tau. \qquad (2)$$

Definition 2: Let $\alpha \in (0,1)$ (Losada and Nieto (Losada and Nieto, 2015). The fractional integral of order α of a function f is defined by:

$$I_\alpha^t f(t) = \frac{2(1-\alpha)}{(2-\alpha)M(\alpha)} f(t) + \frac{2\alpha}{(2-\alpha)M(\alpha)} \int_a^t f(\tau) d\tau, t \geqslant 0. \qquad (3)$$

The fractional integral of Caputo type of function of order $0 < \alpha < 1$, represents an average between function f and its integral of order one. Thus, it implies:

$$\frac{2(1-\alpha)}{(2-\alpha)M(\alpha)} + \frac{2\alpha}{(2-\alpha)M(\alpha)} = 1, \qquad (4)$$

From Eq. (4) this concludes that $M(\alpha) = 2/2 - \alpha, 0 \leqslant \alpha \leqslant 1$

Due to this, (Losada and Nieto (Losada and Nieto, 2015) reformulated the new Caputo derivative of order $0 < \alpha < 1$, as:

$$D_t^\alpha f(t) = \frac{1}{(1-\alpha)} \int_a^t e^{\left(\frac{-\alpha(t-\tau)}{(1-\alpha)}\right)} \frac{\partial f(\tau)}{\partial \tau} d\tau, \qquad (5)$$

Some properties of Caputo-Fabrizio fractional derivative are presented below:

i. For a variable p, the Laplace transform of a Caputo-Fabrizio fractional derivative is:

$$L\{D_t^\alpha f(t)\} = \frac{pL\{f(t) - f(0)\}}{p(1-\alpha) + \alpha}. \qquad (6)$$

ii. The fractional derivative $D_t^{(\alpha+n)}f(t)$ of order $(\alpha + n)$, if $n \geqslant 1$ and $\alpha \in (0,1)$ is given by:

$$D_t^{(\alpha+n)}f(t) = D_t^\alpha(D_t^{(n)}f(t)). \qquad (7)$$

iii. The fractional derivative of the elementary and transcendental functions according to the definition (5), (for $\sin wt$) is given as:

$$D_t^\alpha \sin(\omega t) = \frac{1}{(1-\alpha)} \int_0^t \omega e^{\left(\frac{-\alpha(t-\tau)}{(1-\alpha)}\right)} \cos \omega \tau d\tau. \qquad (8)$$

iv. The Caputo-Fabrizio fractional operator can be extended by letting $\alpha = 1$, in Eq. (6); we get:

$$\lim_{\alpha \to 1} L\{D_t^\alpha f(t)\} = \lim_{\alpha \to 1} L\left[\frac{pL\{f(p) - f(0)\}}{p(1-\alpha) + \alpha}\right] = pL\{f(p) - f(0)\}$$
$$= L\{f\prime(p)\}. \qquad (9)$$

v. If f is infinitely differentiable then, the result obtained is:

$$D_t^\alpha \left[\int_0^t f(t)\right] = \frac{M(\alpha)}{(1-\alpha)} \sum_{n=0}^\infty \frac{f^{(n)}(0) \frac{M(\alpha)}{(1-\alpha)} e^{\left(-\frac{t\alpha}{(1-\alpha)}\right)} nt^n \left(-\frac{t\alpha}{(1-\alpha)}\right)^{-n}}{n!}$$
$$\times \left[\Gamma(n) - \Gamma(n, -\frac{t\alpha}{(1-\alpha)})\right]. \qquad (10)$$

3. Mathematical framework

An unsteady flow of generalized Maxwell fluid with second order slip is taken into consideration over a plate. The fluid covers the area $y^* > 0$ and magnetic field (uniform) is normally applied to the flow. At $t^* = 0$ the plate and fluid are static and the flow starts due to the motion of the plate with velocity $At^{*b}(b > 0)$ at $t^* > 0$. Slip boundary is taken between the velocity of the wall and fluid velocity along with porous medium. Fig. 1 illustrates the physical interpretation of the problem.

The governing equations can be described as:

$$(1 + \lambda^* D_{t^*}^\alpha)\tau^*(y^*, t^*) = \mu \frac{\partial u^*(y^*, t^*)}{\partial y^*}, \qquad (11)$$

$$\rho(1 + \lambda^* D_{t^*}^\alpha)\frac{\partial u^*(y^*, t^*)}{\partial t^*} = \mu \frac{\partial^2 u^*(y^*, t^*)}{\partial y^2} - \sigma B_0^2 \rho(1 + \lambda^* D_{t^*}^\alpha)u^*(y^*, t^*)r$$
$$- \frac{\mu}{\rho k_0}u^*(y^*, t^*) + (1 + \lambda^* D_{t^*}^\alpha)\rho\beta g(T^* - T_\infty), \qquad (12)$$

$$\rho c_p(D_{t^*}^\alpha(y^*, t^*)) = k_1 \left(1 + \frac{16\sigma^* T^3}{3k_1 k^*}\right)\frac{\partial^2 T^*(y^*, t^*)}{\partial y^2}, \qquad (13)$$

Here u^* symbolizes velocity along x direction, T^* is temperature, τ^* is shear stress and $\rho, \beta, \mu, g, \sigma, B_0, \sigma^*, k^*$ are density, thermal expansion coefficient, dynamic viscosity, gravitational force, electrical conductivity, magnetic field factor, Stefan–Boltzman and absorption coefficient respectively. Here k_0 is porosity and k_1 is the thermal conductivity. The boundary conditions are:

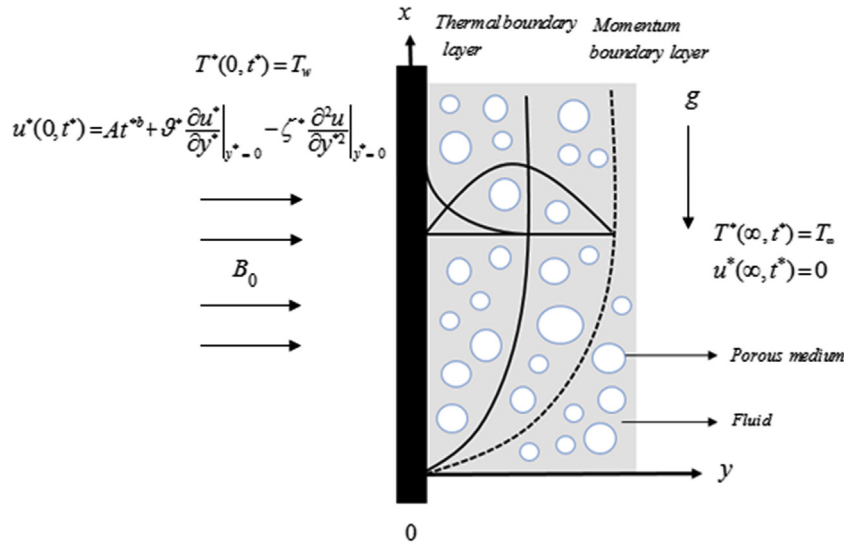$$u(y^*, 0) = \frac{\partial u^*(y^*, 0)}{\partial t^*} = 0 \quad y^* > 0, \qquad (14)$$

Fig. 1. Geometric representation of the problem.

$$u^*(0,t^*) = At^{*b} + \vartheta^* \left.\frac{\partial u^*}{\partial y^*}\right|_{y^*=0} - \zeta^* \left.\frac{\partial^2 u}{\partial y^2}\right|_{y^*=0}, \tag{15}$$

$$u^*(y^*,t^*), \frac{\partial u^*(y^*,t^*)}{\partial y^*} \to 0; y^* \to \infty, \quad t^* > 0 \tag{16}$$

$$T^*(y^*,0) = T_\infty,$$
$$T^*(0,t^*) = T_w,$$
$$T^*(y^*,t^*) = T_\infty, \quad y^* \to \infty \tag{17}$$

where ϑ^*, $zeta^*$, is first and second order slip parameters respectively. We utilize the following dimensionless variables in the governing equations:

$$u = \frac{u^*}{(Av^b)^{\frac{1}{2b+1}}}, y = \frac{y^*(Av^b)^{\frac{1}{2b+1}}}{v}, t = \frac{t^*(Av^b)^{\frac{2}{2b+1}}}{v}, M = \frac{M^*v}{(Av^b)^{\frac{2}{2b+1}}},$$

$$\lambda = \lambda^* \left(\frac{(Av^b)^{\frac{2}{2b+1}}}{v}\right)^\alpha, \vartheta = \frac{\vartheta^*(Av^b)^{\frac{1}{2b+1}}}{v}, \zeta = \frac{\zeta^*(Av^b)^{\frac{2}{2b+1}}}{v^2}, \tag{18}$$

$$\tau = \frac{\tau^*}{\rho(Av^b)^{\frac{2}{2b+1}}}, \theta = \frac{T^* - T_\infty}{T_w - T_\infty}.$$

After non-dimensionalization, Eqs. (11)–(13) may be written as:

$$(1 + \lambda D_t^\alpha)\tau(y,t) = \frac{\partial u(y,t)}{\partial y}, \tag{19}$$

$$(1 + \lambda D_t^\alpha)\frac{\partial u(y,t)}{\partial t} = \frac{\partial^2 u(y,t)}{\partial y^2} - M(1 + \lambda D_t^\alpha)u(y,t) - Ku(y,t)$$
$$+ (1 + \lambda D_t^\alpha)Gr\theta, \tag{20}$$

$$Pr_{eff}\frac{\partial^\alpha \theta}{\partial t^\alpha} = \frac{\partial^2 \theta}{\partial y^2}, \tag{21}$$

where

$$M = \sigma B_0^2 \rho, Gr = \frac{\gamma\beta g(T_w - T_\infty)}{(Av^b)^{\frac{3}{2b+1}}}, Nr = \frac{16\sigma T_\infty^3}{3k_1 k^*},$$

$$K = \frac{v^2}{k_0(Av^b)^{\frac{2}{2b+1}}}, Pr = \frac{\mu c_p}{k_1}, Pr_{eff} = \frac{Pr}{1 + Nr},$$

are magnetic parameter, Grashoff number, radiation parameter, porosity parameter and effective Prandtl number. Eqs. (15)-(17) become:

$$u(y,0) = \frac{\partial u(y,0)}{\partial t} = 0 \quad y > 0, \tag{22}$$

$$u(0,t) = t^b + \vartheta \left.\frac{\partial u}{\partial y}\right|_{y=0} - \zeta \left.\frac{\partial^2 u}{\partial y^2}\right|_{y=0}, \tag{23}$$

$$u(y,t), \frac{\partial u(y,t)}{\partial y} \to 0; y \to \infty, t > 0, \tag{24}$$

$$\theta(y,0) = 0,$$
$$\theta(0,t) = 1,$$
$$\theta(y,t) = 0, \quad y \to \infty. \tag{25}$$

4. Method of solution

The fractional differential equations are solved via semi analytical Laplace transform technique. Numerical inverse Laplace transform technique is applied to acquire the solutions of temperature, velocity and shear stress. Let us define $L\{u(y,t)\} = \bar{u}y,s)$, and s denotes the transform parameter.

4.1. Temperature

Applying Laplace transform to Eq. (21) and using Eq. (25), we acquire:

$$Pr_{eff}s^\alpha \bar{\theta}(y,s) = \frac{\partial^2 \bar{\theta}(y,s)}{\partial y^2} \tag{26}$$

$$\bar{\theta}(0,s) = 0, \bar{\theta}(1,s) = \frac{1}{s}, \tag{27}$$

with solution:

$$\bar{\theta}(y,s) = \frac{1}{s}e^{-y\sqrt{\frac{Pr_{eff}\, gammas}{s+alphagamma}}}, \tag{28}$$

with its inverse Laplace transform for $0 < \alpha < 1$

$$\theta(y,t) = 1 - \frac{2Pr_{eff}\gamma}{\pi}\int_0^\infty \frac{\sin yx}{qPr_{eff}\gamma + q^2}e^{-\frac{\alpha\gamma tq^2}{Pr_{eff}\gamma + q}}dq, \qquad (29)$$

where $\gamma = \frac{1}{1-\alpha}$. The Nusselt number is evaluated as:

$$Nu = -\frac{\partial\theta(y,t)}{\partial y}\Big|_{y=0} = -L^{-1}\left\{\frac{\partial\bar\theta(y,s)}{\partial y}\Big|_{y=0}\right\},$$

$$= -L^{-1}\left\{\frac{1}{s}\sqrt{\frac{Pr_{eff}\gamma s}{s+\alpha\gamma}}\right\} = \sqrt{Pr_{eff}\gamma}I_0(\frac{\alpha\gamma}{2}t)e^{-(\frac{\alpha\gamma}{2}t)}, 0 < \alpha < 1. \qquad (30)$$

4.2. Velocity

Applying Laplace transform to Eq. (20) and using Eqs. (22)–(24), we obtain:

$$\frac{\partial^2\bar u(y,s)}{\partial y^2} - ((s+M)(1+\lambda s^\alpha)+K)\bar u(y,s) = -(1+\lambda s^\alpha)Gr\bar\theta(y,s), \qquad (31)$$

4.3. Subject to the boundary conditions

$$u(0,t) = \frac{1}{s^b+1} + \vartheta\frac{\partial\bar u}{\partial y}\Big|_{y=0} - \zeta\frac{\partial^2\bar u}{\partial y^2}\Big|_{y=0}, \qquad (32)$$

$$\bar u(y,s), \frac{\partial\bar u(y,s)}{\partial y} \to 0; y \to \infty, \qquad (33)$$

$$\bar u(y,s) = \frac{\left\{\frac{1}{s^b+1} - \vartheta\frac{1}{s}A\sqrt B + \zeta\frac{1}{s}AB - \frac{A}{s}\right\}}{\left\{1 + \vartheta\sqrt C + \zeta C\right\}}e^{-y\sqrt C}$$
$$- \frac{(1+\lambda s^\alpha)Gr}{s(B + (1+\lambda s^\alpha)\sqrt B - M(1+\lambda s^\alpha) - K)}e^{-y\sqrt B}, \qquad (34)$$

where

$$A = -\frac{(1+\lambda s^\alpha)Gr}{\left(\frac{Pr_{eff}\gamma s}{s+\alpha\gamma} + (1+\lambda s^\alpha)\sqrt{\frac{Pr_{eff}\gamma s}{s+\alpha\gamma}} - M(1+\lambda s^\alpha) - K\right)}, \quad B = \frac{Pr_{eff}\gamma s}{s+\alpha\gamma},$$
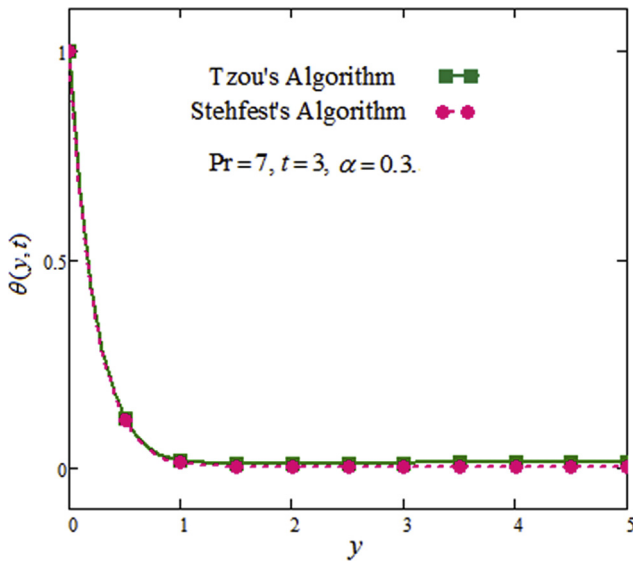
$$C = ((s+M)(1+\lambda s^\alpha) + K)$$

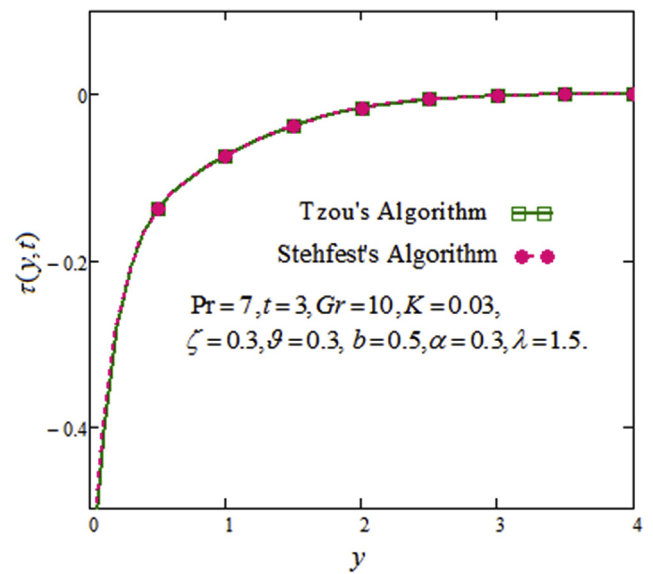**Fig. 2.** Temperature profile comparison for Tzou's and Stehfest's algorithm.

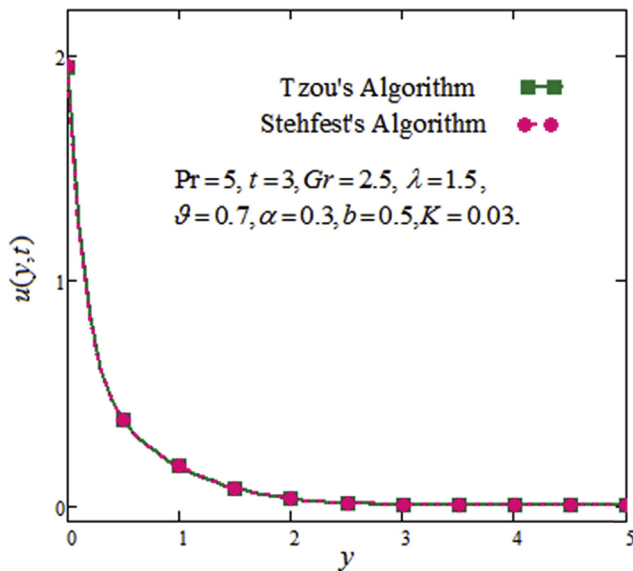**Fig. 4.** Shear stress profile comparison for Tzou's and Stehfest's algorithm.

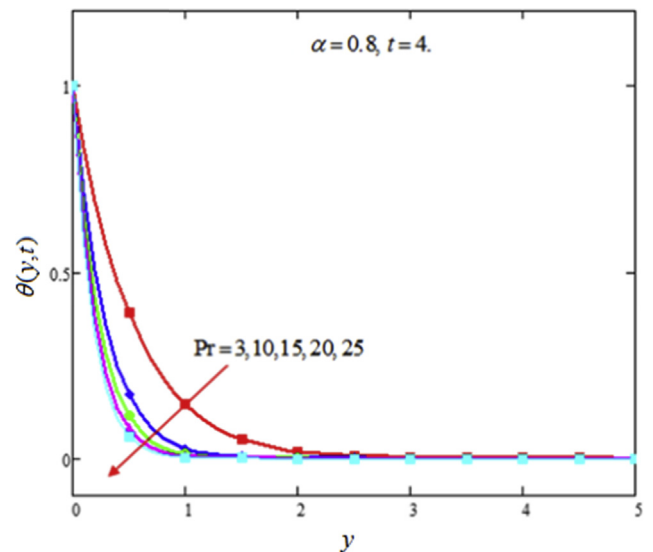**Fig. 3.** Velocity profile comparison for Tzou's and Stehfest's algorithm.

Fig. 5. Temperature profile for variation of Prandtl number Pr.

.

Taking Laplace transform of Eq. (14), the shear stress in transform domain can be expressed as:

$$\bar{\tau}(y,s) = -\frac{1}{(1+\lambda s^\alpha)}\left\{ \frac{\sqrt{C}\{\frac{1}{s^b+1} - \vartheta\frac{1}{s}A\sqrt{B} + \zeta\frac{1}{s}AB - \frac{A}{s}\}}{\{1+\vartheta\sqrt{C}+\zeta C\}}e^{-y\sqrt{C}} \right.$$
$$\left. -\frac{\sqrt{B}(1+\lambda s^\alpha)Gr}{s(B+(1+\lambda s^\alpha)\sqrt{B} - M(1+\lambda s^\alpha) - K)}e^{-y\sqrt{B}} \right\}. \quad (35)$$

Due to complexity of Eqs. (24) and (35), we use numerical Inverse Laplace transform using Stehfest's algorithm (Stehfest, 1970) and compared with Tzou's algorithm (Tzou and Puri, 1997). The solution for Stehfest's algorithm is:

$$u(y,t) = \frac{\ln(2)}{t}\sum_{j=1}^{2n}\left[\left((-1)^{j+n}\sum_{l=floor\left(\frac{j+1}{2}\right)}^{\frac{(j+n)-|j-n|}{2}}\left[\frac{i^n(2l)}{(n-1)l(l-1)(j-1)(2l-j)}\right]\bar{u}\right.\right.$$
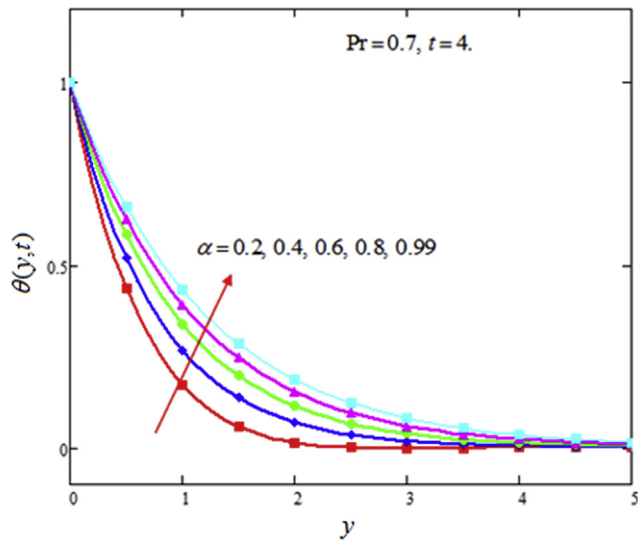$$\left.\left(y,\frac{j\ln(2)}{t}\right)\right)\right], \quad (36)$$

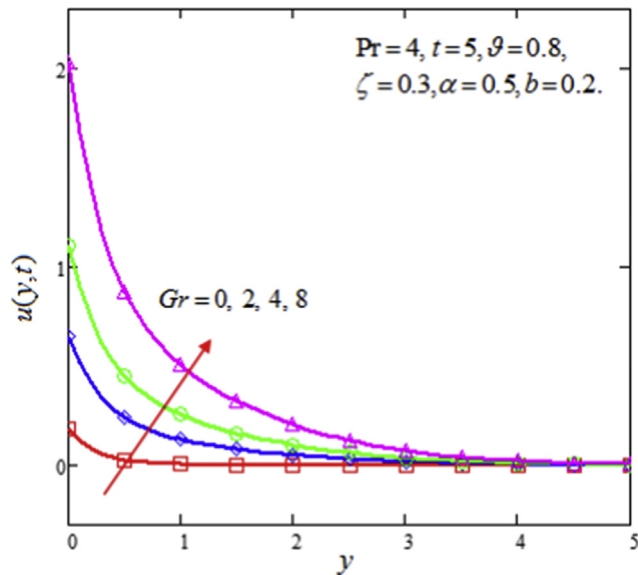**Fig. 6.** Temperature profile for variation of fractional parameter α.

Fig. 7. Velocity profile for variation of Grashoff number *Gr*.

where the parameter *n* is called "Stehfest number" and should be even. The solution for Tzou's algorithm is given as:

$$u(y,t) = \frac{e^{4.7}}{2}\left(\frac{\bar{u}(y,\frac{4.7}{t})}{2} + \text{Re}\left(\sum_{q=1}^{N1}(-1)^q\bar{u}\left(y,\frac{4.7+n\pi i}{t}\right)\right)\right). \quad (37)$$

where N_1 is a natural number ($N_1 \gg 1$), Re(·) denotes the real part and *i* is the imaginary unit (Stehfest, 1970).

5. Results and discussion

In the present study, heat transfer flow of a generalized Maxwell fluid with magnetic force, porosity and second order slip effects are inspected. The problem is modeled in terms of coupled PDEs. Some non-dimensional variables are introduced to transform
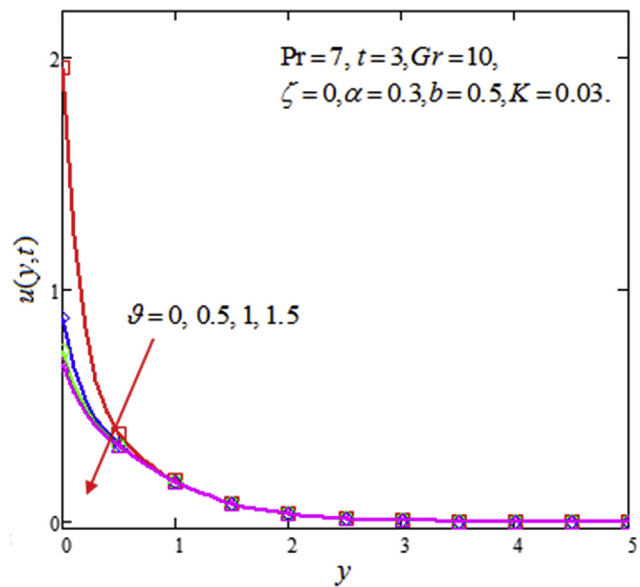

Fig. 8. Velocity profile for variation of first order slip parameter ϑ.

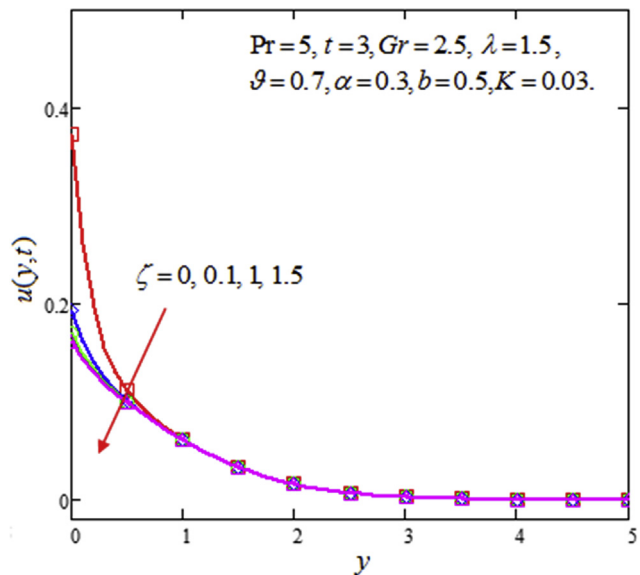**Fig. 9.** Velocity profile for variation of second order slip parameter ζ.

the PDEs to ordinary differential equations. Semi analytical and numerical Inverse Laplace transform technique is used to solve the problem. Graphical and tabular comparison between the two algorithms is made. Effect of various parameters is presented via graphs.

In (Figs. 2–4), the present results for solution of velocity and shear stress obtained via Stehfest's and Tzou's algorithms are compared. Both graphs show the validation of the present results. Here we choose to use Stehfest's algorithm for our results as this algorithm is highly accurate and stable Method which is widely used in engineering.

Fig. 5 depicts the impact of Prandtl number, Pr, on the temperature of fluid for Stehfest's algorithm. The temperature is decreasing function of Pr. Physically, the increase in Prandtl number minimizes viscosity which reduces thermal boundary layer. Fig. 6 illustrates the impact of fractional parameter, α, on the tempera-

ture field for Stehfest's algorithm. The result obtained shows that increasing fractional parameter values leads to an increase in temperature of the fluid.

Fig. 7 depicts the behavior of velocity field with varying Grashoff number for Stehfest's algorithm. Velocity field is an increasing function of Grashoff number due to dominant buoyancy force. The velocity field is zero at $Gr = 0$, showing that the fluid flows due to buoyancy force. Fig. 8 shows that velocity field is a decreasing function of first order slip parameter, ϑ. The fluid velocity is lowest for highest value of first order slip parameter.

Fig. 9 explains velocity behavior with varying second order slip parameter, ζ. Velocity of the fluid reduces with maximizing values of ζ. Physically, reducing fluid velocity means Maxwell fluid's viscosity increases. The impact of fractional parameter on the velocity profile are shown in Fig. 10. The velocity of Maxwell fluid decreases with the increasing fractional parameter. Increasing value of
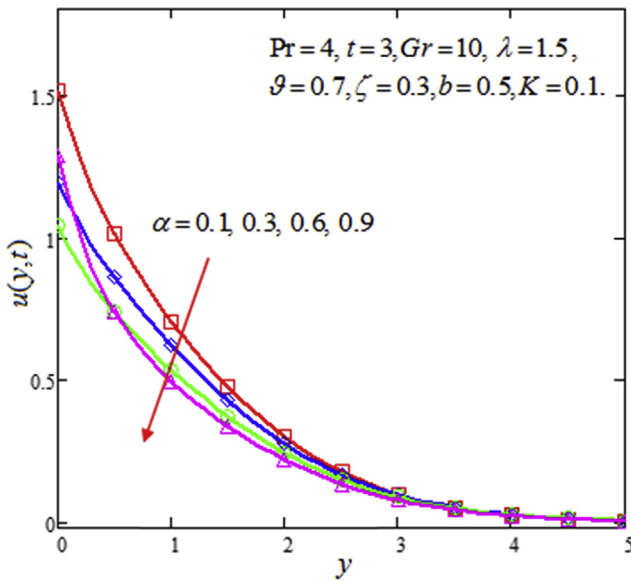

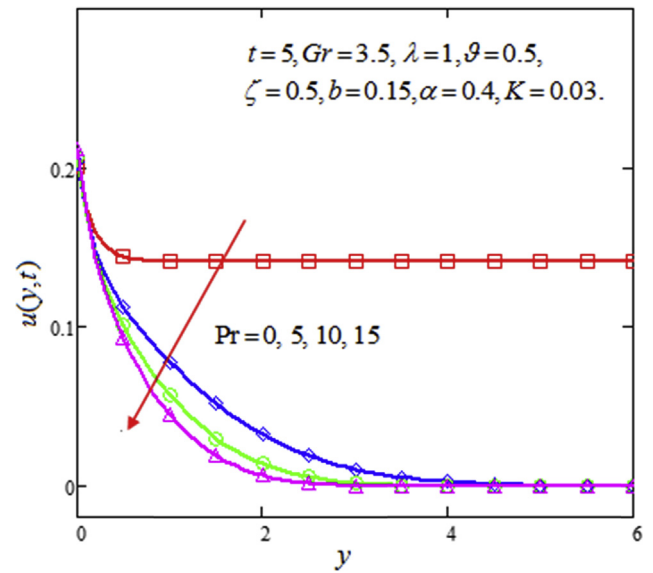**Fig. 10.** Velocity profile for variation of fractional parameter α.

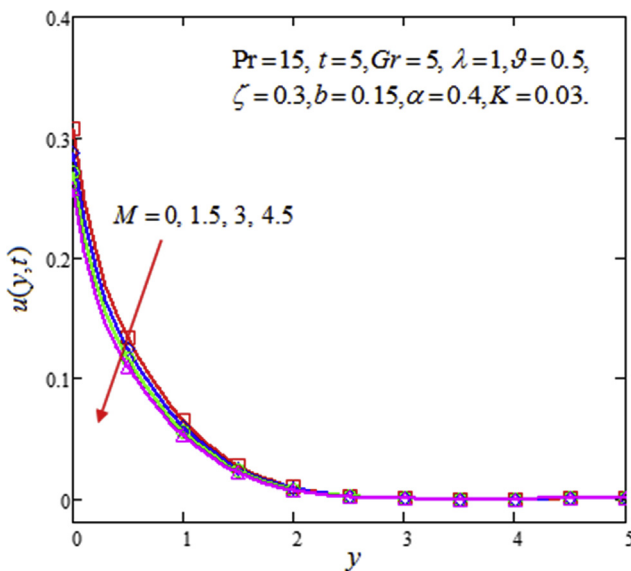**Fig. 12.** Velocity profile for variation of Prandtl number Pr.

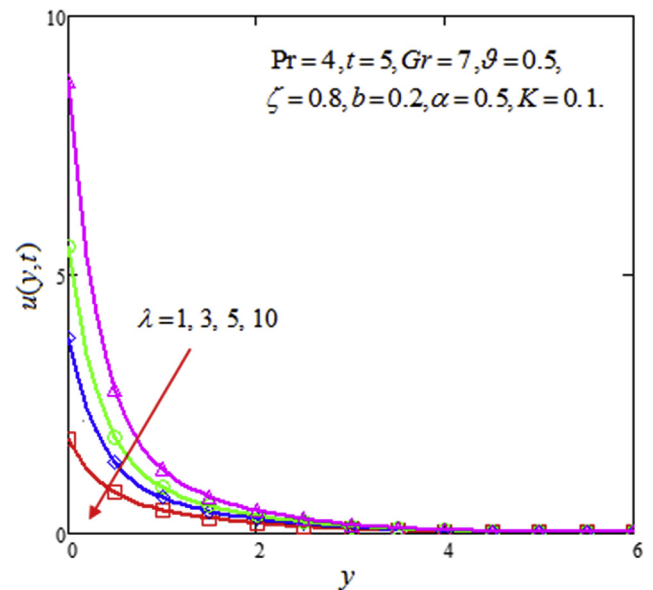**Fig. 11.** Velocity profile for variation of Magnetic parameter M.

Fig. 13. Velocity profile for variation of relaxation time λ.

fractional parameter increases viscosity of fluids which leads to decrease the velocity of the fluid. Fig. 11 illustrates the impact of magnetic parameter, M on velocity profile. The increasing M tends to decrease the velocity profile. The magnetic force (produced due to external applied magnetic field) opposes velocity of the fluid. The graph for Prandtl number for both algorithms is sketched in Fig. 12. Prandtl number, Pr, one of the important parameter in fluid dynamics, is the ratio of momentum to thermal diffusivity. Velocity of fluid minimizes with increasing Prandtl number and has greater velocity at zero Prandtl number. Momentum diffusivity becomes dominant than thermal diffusivity when Prandtl number increases. Therefore, momentum diffusivity leads to decrease the fluid velocity.

Fig. 13 depicts the variation of fluid velocity with relaxation time, λ. Velocity shows the same decreasing behavior with increas-ing values of relaxation time. Fig. 14 illustrates that velocity of the fluid maximizes with increasing porosity parameter. The greater the porosity parameter is, the faster the fluid flows. Figs. 15 and 16 depict the impact of variation of M on velocity of the fluid for constant values ($K = 0.03$) and ($K = 0.04$) respectively. The veloc-ity decreases with increasing magnetic effects and the fluid veloc-ity is greater for ($K = 0.04$) compared to ($K = 0.03$). Figs. 17 and 18 illustrate the variation of fluid velocity with variation of porosity parameter, K, while considering maximum and minimum values for magnetic parameter, ($M = 0.5$) and ($M = 3$). The fluid flows fas-ter at ($M = 0.5$) while the velocity is lower under greater effect of magnetic field with ($M = 3$), as the magnetic forces retard the fluid flow.

The variation of shear stress with first order slip parameter, ϑ, is shown in Fig. 19. The shear stress is increasing function of ϑ. Fig. 19
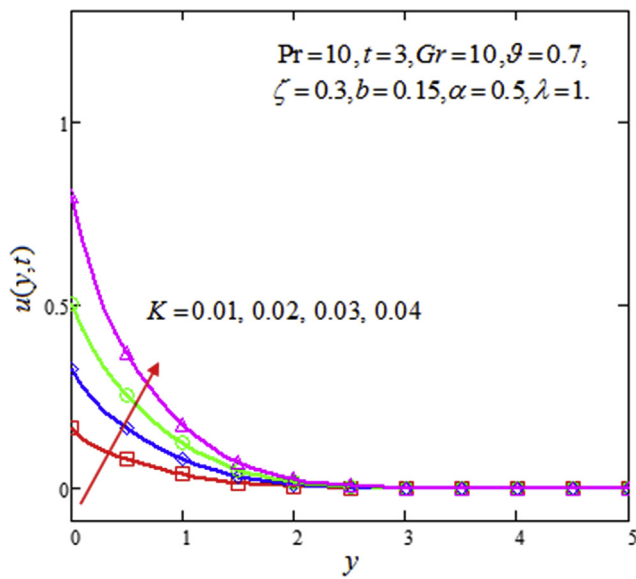

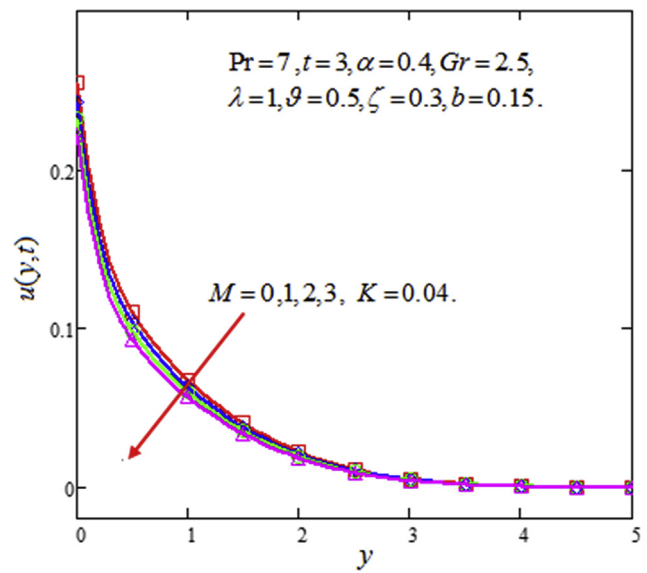**Fig. 14.** Velocity profile for variation of porosity parameter K.

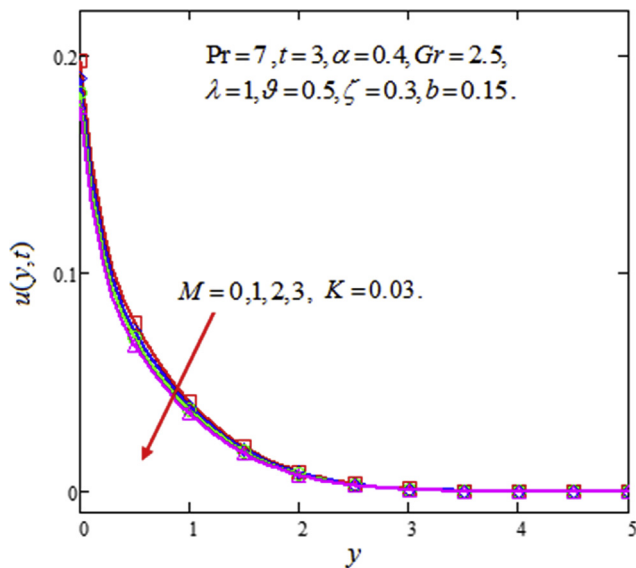**Fig. 16.** Velocity profile for variation of magnetic parameter M for constant $K = 0.04$.

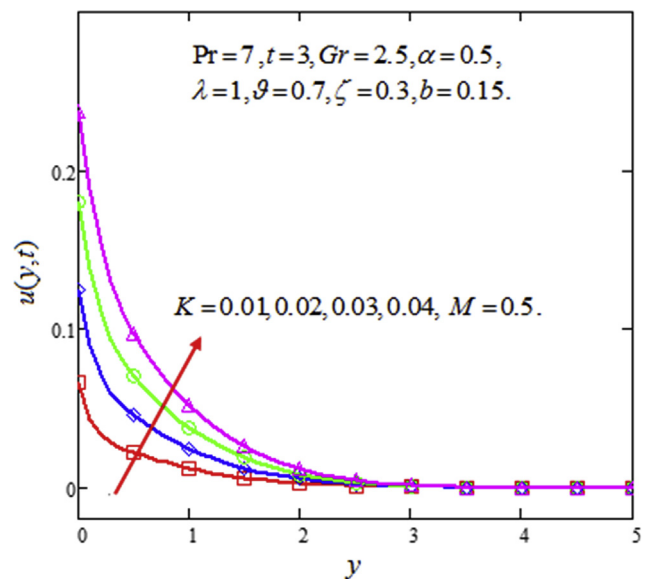**Fig. 15.** Velocity profile for variation of magnetic parameter M for constant $K = 0.03$.

Fig. 17. Velocity profile for variation of porosity parameter K for constant $M = 0.5$.
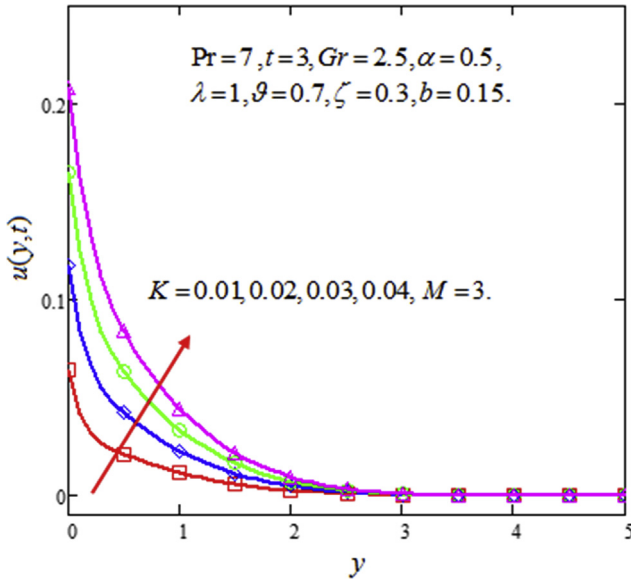
Fig. 18. Velocity profile for variation of porosity parameter K for constant $M = 3$.
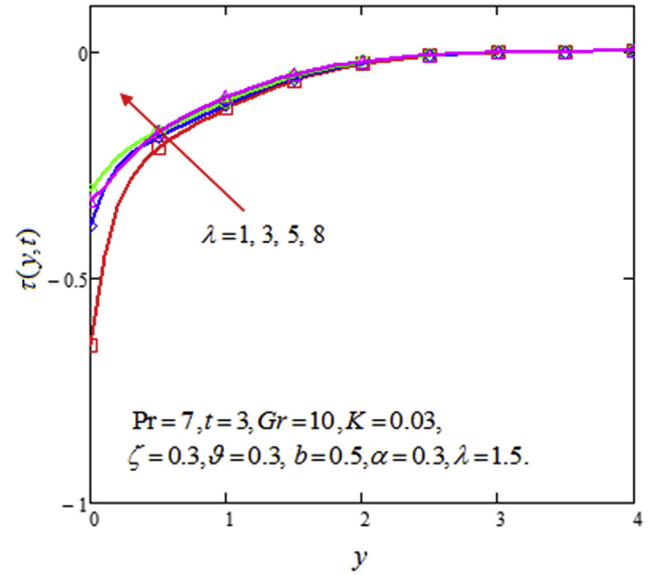

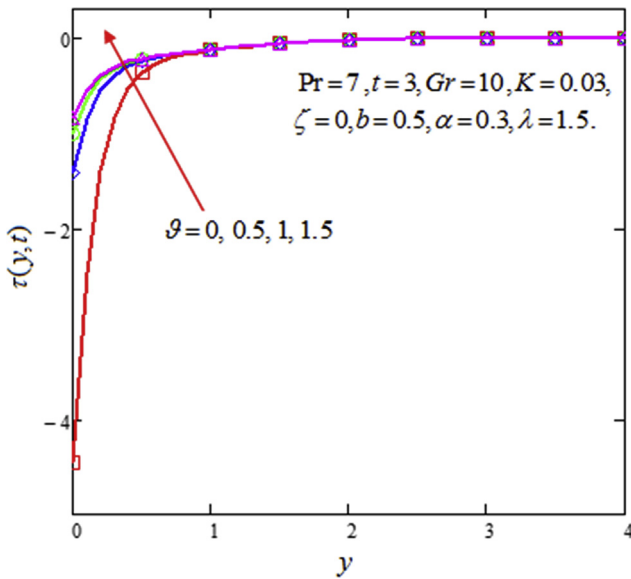**Fig. 20.** Shear stress profile for variation of relaxation time λ.

Fig. 19. Shear stress profile for variation of first order slip parameter ϑ.
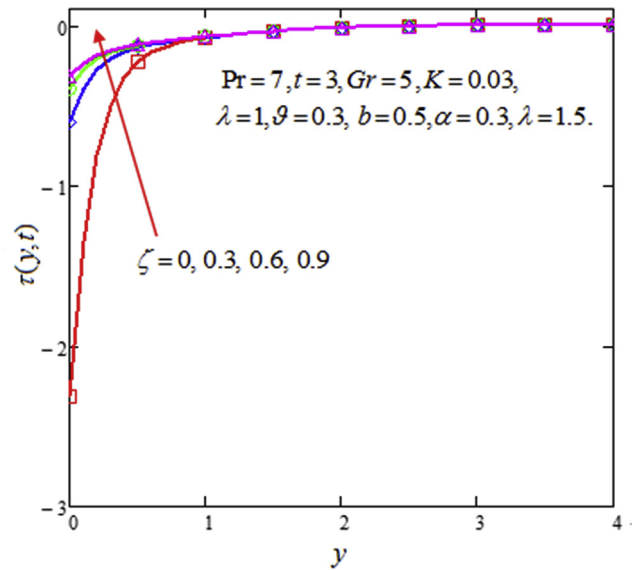

Fig. 21. Shear stress profile for variation of second order slip parameter ζ.

shows that shear stress is smaller in the absence of first order slip parameter, ϑ. Fig. 20 depicts the behavior of shear stress with variation in relaxation time. The shear stress is increasing with increasing relaxation time in the presence of slip parameters. The variation is significant near the plate while at some distance from the plate there is no change in the shear stress. Fig. 21 depicts that shear stress is an increasing function of second order slip parameter in the presence of first order slip parameter. Moreover, shear stress is smaller in the absence of second order slip parameter, ζ, while maximizes with increasing values of ζ. This variation is effective near the plate and after $y = 1$, there is no variation in the shear stress. The numerical comparison for temperature is presented in Table 1 for the sake of validation while numerical comparison for velocity solution is shown in Table 2 at various distances of the plate. To establish the validation for shear stress,

Table 1
Comparison of numerical inverse laplace transform for temperature by Stehfest's and Tzou's algorithm.

y	0	0.1	0.2	0.3	0.4	0.5	0.6
$\theta(y,t)$[Stehfest's]	1	0.662	0.434	0.28	0.182	0.0117	0.075
$\theta(y,t)$ [Tzou's]	1	0.661	0.432	0.28	0.18	0.0114	0.072

Table 2
Numerical inverse Laplace transform for velocity by Stehfest's and Tzou's algorithm.

y	0	0.1	0.2	0.3	0.4	0.5	0.6
$u(y,t)$ [Stehfest's]	1.949	1.24	0.842	0.608	0.46	0.38	0.318
$u(y,t)$ [Tzou's]	1.954	1.23	0.832	0.603	0.46	0.38	0.318

Table 3
Numerical inverse Laplace transform for shear stress by Stehfest's and Tzou's algorithm.

y	0	0.1	0.2	0.3	0.4	0.5	0.6
$u(y,t)$ [Stehfest's]	−0.607	−0.406	−0.81	−0.505	−0.331	−0.231	−0.171
$u(y,t)$ [Tzou's]	−0.601	−0.40	−0.811	−0.506	−0.332	−0.231	−0.172

a comparison is made in Table. 3. It is concluded that the results are validated through these illustrations.

6. Conclusion

In this study, a generalized Maxwell fluid with second order slip effect is investigated and the problem was solved via Laplace transform and Numerical Inverse Laplace transform. The solution is compared for two numerical algorithms namely Tzou's and Stehfest's algorithms and we choose Stehfest's algorithm to solve the problem. Furthermore, the results are illustrated via graphs and we concluded that velocity and shear stress are smaller in the presence of slip parameters. The Fluid flow increases gradually with porosity parameter. For the sake of accuracy, we compared the results of two algorithms graphically and numerically for temperature, velocity and shear stress.

Acknowledgment

References

Abbas, Z., Sajid, M., Hayat, T., 2006. MHD boundary-layer flow of an upper-convected Maxwell fluid in a porous channel. Theor. Comput. Fluid Dynam. 20 (4), 229–238.

Abbasbandy, S., Hayat, T., Alsaedi, A., Rashidi, M.M., 2014. Numerical and analytical solutions for falkner-skan flow of MHD oldroyd-B fluid. Int. J. Numer. Methods Heat Fluid Flow 24 (2), 390–401.

Abbasi, A., Ahmad, I., Ali, N., Hayat, T., 2016. An analysis of peristaltic motion of compressible convected Maxwell fluid. AIP Adv. 6, (1) 015119.

Abdeljawad, T., Baleanu, D., 2016. Discrete fractional differences with nonsingular discrete Mittag-Leffler kernels. Adv. Differ. Equati. 1, 232.

Abdeljawad, T., Baleanu, D., 2016. Discrete fractional differences with nonsingular discrete Mittag-Leffler kernels. Adv. Differ. Equat. 1, 232.

Abdeljawad, T., Baleanu, D., 2017. On fractional derivatives with exponential kernel and their discrete versions. Rep. Mathemat. Phys. 80 (1), 11–27.

Abu-Saris, R., Al-Mdallal, Q.M., 2013. On the asymptotic stability of linear system of fractional-order difference equations. Fract. Calculus Appl. Anal. 16 (3), 613–629.

Agarwal, P., Jain, S., Mansour, T., 2017. Further extended Caputo fractional derivative operator and its applications. Russ. J. Mathemat. Phys. 24 (4), 415–425.

Al-Mdallal, Q.M., Hajji, M.A., 2015. A convergent algorithm for solving higher-order nonlinear fractional boundary value problems. Fract. Calculus Appl. Anal. 18 (6), 1423–1440.

Al-Mdallal, Q.M., Syam, M.I., 2012. An efficient method for solving non-linear singularly perturbed two points boundary-value problems of fractional order. Commun. Nonlinear Sci. Numer. Simul. 17 (6), 2299–2308.

Al-Mdallal, Q.M., Syam, M.I., Anwar, M.N., 2010. A collocation-shooting method for solving fractional boundary value problems. Commun. Nonlinear Sci. Numer. Simulat. 15 (12), 3814–3822.

Aman, S., Khan, I., Ismail, Z., Salleh, M.Z., Al-Mdallal, Q.M., 2017a. Heat transfer enhancement in free convection flow of CNTs Maxwell nanofluids with four different types of molecular liquids. Sci. Rep. 7 (1), 2445.

Aman, S., Salleh, M.Z., Ismail, Z., Khan, I., 2017b. Exact solution for heat transfer free convection flow of Maxwell nanofluids with graphene nanoparticles. J. Phys. Confer. Ser. 890, (1). IOP Publishing 012004.

Aman, S., Khan, I., Ismail, Z., Salleh, M.Z., Tlili, I., 2018b. A new Caputo time fractional model for heat transfer enhancement of water-based graphene nanofluid: an application to solar energy. Results Phys. 9, 1352–1362.

Aman, S., Khan, I., Ismail, Z., Salleh, M.Z., 2018a. Applications of fractional derivatives to nanofluids: exact and numerical solutions. Mathemat. Modell. Nat. Phenom. 13 (1).

Atangana, A., 2016. On the new fractional derivative and application to nonlinear Fisher's reaction–diffusion equation. Appl. Mathemat. Comput. 273, 948–956.

Baltaeva, U., Agarwal, P., 2018. Boundary-value problems for the third-order loaded equation with non-characteristic type-change boundaries. Mathemat. Methods Appl. Sci. 41 (9), 3307–3315.

Caputo, M., Fabrizio, M., 2015. A new definition of fractional derivative without singular kernel. Progr. Fract. Differ. Appl. 1 (2), 1–13.

Day, M.A., 1990. The no-slip condition of fluid dynamics. Erkenntnis 33 (3), 285–296.

Ebaid, A., 2008. Effects of magnetic field and wall slip conditions on the peristaltic transport of a Newtonian fluid in an asymmetric channel. Phys. Lett. A 372 (24), 4493–4499.

Fetecau, C., Athar, M., Fetecau, C., 2009. Unsteady flow of a generalized Maxwell fluid with fractional derivative due to a constantly accelerating plate. Comput. Mathemat. Appl. 57 (4), 596–603.

Fetecau, C., Fetecau, C., 2004. Unsteady helical flows of a Maxwell fluid. Proc. Romanian Acad. Ser. A 5 (1), 13–19.

Hayat, T., Sajjad, R., Abbas, Z., Sajid, M., Hendi, A.A., 2011. Radiation effects on MHD flow of Maxwell fluid in a channel with porous medium. Int. J. Heat Mass Trans. 54 (4), 854–862.

Hayat, T., Shafiq, A., Alsaedi, A., Shahzad, S.A., 2016. Unsteady MHD flow over exponentially stretching sheet with slip conditions. Appl. Mathemat. Mech. 37 (2), 193–208.

Hsiao, K.L., 2014. Conjugate heat transfer for mixed convection and Maxwell fluid on a stagnation point. Arab. J. Sci. Eng. 39 (6), 4325–4332.

Hsiao, K.L., 2017. Combined electrical MHD heat transfer thermal extrusion system using Maxwell fluid with radiative and viscous dissipation effects. Appl. Ther. Eng. 112, 1281–1288.

Ishak, N., Hashim, H., Mohamed, M.K.A., Sarif, N.M., Rosli, N., Salleh, M.Z., 2017. Thermal radiation effects on stagnation point flow past a stretching/shrinking sheet in a Maxwell fluid with slip condition. J. Phys. Confer. Ser. 890 (1), 012021. IOP Publishing.

Jamil, M., Rauf, A., Zafar, A.A., Khan, N.A., 2011. New exact analytical solutions for Stokes' first problem of Maxwell fluid with fractional derivative approach. Comput. Math. Appl. 62 (3), 1013–1023.

Liu, Y., Guo, B., 2017. Effects of second-order slip on the flow of a fractional Maxwell MHD fluid. J. Assoc. Arab Univ. Basic Appl. Sci. 24, 232–241.

Losada, J., Nieto, J.J., 2015. Properties of a new fractional derivative without singular kernel. Progr. Fract. Differ. Appl. 1 (2), 87–92.

Ruzhansky, M., Cho, Y.J., Agarwal, P., 2017. Advances in Real and Complex Analysis with. Applications. Springer Singapore.

Shah, N.A., Zafar, A.A., Fetecau, C., 2017. Free convection flows over a vertical plate that applies shear stress to a fractional viscous fluid. Alex. Eng. J.

Siddique, I., Vieru, D., 2011. Stokes flows of a Newtonian fluid with fractional derivatives and slip at the wall. Int. Rev. Chem. Eng. 3 (6), 822–826.

Stehfest, H., 1970. Algorithm 368: numerical inversion of Laplace transforms [D5]. Commun. ACM 13 (1), 47–49.

Tahir, M., Imran, M.A., Raza, N., Abdullah, M., Aleem, M., 2017. Wall slip and non-integer order derivative effects on the heat transfer flow of Maxwell fluid over an oscillating vertical plate with new definition of fractional Caputo-Fabrizio derivatives. Results Phys. 7, 1887–1898.

Tan, W., Masuoka, T., 2007. Stability analysis of a Maxwell fluid in a porous medium heated from below. Phys. Lett. A 360 (3), 454–460.

Tripathi, D., Bég, O.A., 2012. A numerical study of oscillating peristaltic flow of generalized Maxwell viscoelastic fluids through a porous medium. Trans. Porous Media 95 (2), 337–348.

Tzou, D.Y., Puri, P., 1997. Macro-to microscale heat transfer: the lagging behavior. Appl. Mech. Rev. 50, B82.

Vieru, D., Rauf, A., 2011. Stokes flows of a Maxwell fluid with wall slip condition. Can. J. Phys. 89 (10), 1061–1071.

Vieru, D., Zafar, A.A., 2013. Some couette flows of a Maxwell fluid with wall slip condition. Appl. Math. Inf. Sci. 7, 209–219.